Vector-Sum Method for 2D Slope Stability Analysis Considering Vector Characteristics of Force

Mingwei Guo, Ph.D.[1]; Chunguang Li, Ph.D.[2]; Shuilin Wang, Ph.D.[3]; Shunde Yin, Ph.D., M.ASCE[4]; Sujin Liu, Ph.D.[5]; and Xiurun Ge[6]

Abstract: The vector-sum method (VSM) is advanced by considering the vector characteristics. As a cost of this advantage, a predefined global sliding direction is required, which has been a key issue for the application of the VSM. Although the VSM has been steadily refined since its initial version in 2008, limited progress on this issue has been achieved, and the global sliding direction is still prespecified by assumption. In the aim of solving this issue, this article proposes a rigorous analytical solution based on the principle of potential energy minimization. In addition, the VSM is improved by comparing the resisting moment with the driving moment at the moment center, which can be determined by the shape of the slip surface. Finally, this method is verified to be feasible by three classical earthen slopes with different soil composition. Compared with the solutions found by the rigorous Morgenstern-Price method with the half-sine function as the interslice force function, the calculated results demonstrate that the proposed method can accurately estimate slope stability. **DOI: 10.1061/(ASCE)GM.1943-5622.0001436.**

Author keywords: Vector-sum method; Slope stability analysis; Limit equilibrium method; Finite-element method.

Introduction

Slope stability problems focus on the safety factor and the corresponding critical slip surface. Many methods have been developed to perform slope stability analyses, including the conventional limit-equilibrium method (LEM) (Bishop 1955; Morgenstern and Price 1965; Spencer 1967; Janbu 1973; Fredlund and Krahn 1977), the strength-reduction method (SRM) (Zienkiewicz et al. 1975; Griffiths and Lane 1999), and the limit-analysis method (LAM) (Sloan 2013). To date, the LEM and the SRM are the most widely used in practical slope engineering. Considering the sliding body as rigid body, LEMs divide the sliding body into many slices, and many assumptions are made to make the stability problem statically determinate. Based on the limit state of the slices, the safety factor can be iteratively computed under these assumptions, which focus on the magnitude, the direction, and the position of forces acting on the interface of slices (Zhu et al. 2003; Chakraborty and Goswami 2016). Moreover, for three-dimensional (3D) problems, more assumptions are required than in the two-dimensional (2D) method, and an accurate safety factor of the slope can be obtained using a rigorous 3D LEM satisfying all six equilibrium conditions of the sliding body (e.g., Zhu and Qian 2007; Zheng 2012; Zhou and Chen 2013). However, the safety factor obtained by nonrigorous methods satisfying partial equilibrium conditions of the sliding body may be not accurate enough to meet the engineering requirements (e.g., Lam and Fredlund 1993; Cheng and Yip 2007). Therefore, scholars and engineers performing slope stability analyses must have a thorough mastery of soil mechanics and soil strength and the ability and patience to test and judge the results of their analyses in order to avoid mistakes and misuse (e.g., Duncan 1996).

For the widespread finite-element (FE) method in slope stability analysis, there are several methods to compute the safety factor. The popular one is the strength-reduction method (SRM). This method was used early on by Zienkiewicz et al. (1975), and it has since made great progress over the world (e.g., Cheng et al. 2007; Shen and Karakus 2014). Although the SRM can simply and automatically locate the critical slip surface, the inherent theoretical defects in the SRM will yield a result that is not reliable enough (e.g., Tang et al. 2016), which cannot guarantee that the safety factor with its corresponding slip surface is the global optimal solution rather than a suboptimal solution and tends to reach premature nonconvergence under some complex conditions.

In addition to the SRM, there are three other ways of defining the safety factor and finding the critical slip surface based on the stress of the sliding body, and the most popular definition of the safety factor is based on the strength along the slip surface (e.g., Zou et al. 1995; Stianson et al. 2011). These methods find the critical slip

[1]Associate Professor, State Key Laboratory of Geomechanics and Geotechnical Engineering, Wuhan Institute of Rock and Soil Mechanics, Chinese Academy of Science, Xiaohongshan, Wuchang, Wuhan 430071, China (corresponding author). Email: mwguo@whrsm.ac.cn

[2]Associate Professor, State Key Laboratory of Geomechanics and Geotechnical Engineering, Wuhan Institute of Rock and Soil Mechanics, Chinese Academy of Science, Xiaohongshan, Wuchang, Wuhan 430071 China. Email: cgli@whrsm.ac.cn

[3]Professor, State Key Laboratory of Geomechanics and Geotechnical Engineering, Wuhan Institute of Rock and Soil Mechanics, Chinese Academy of Science, Xiaohongshan, Wuchang, Wuhan 430071, China. Email: slwang@whrsm.ac.cn

[4]Associate Professor, Univ. of Waterloo, Dept. of Civil and Environmental Engineering, Waterloo, ON, Canada N2L3G1. Email: shunde.yin@uwaterloo.ca

[5]State Key Laboratory of Geomechanics and Geotechnical Engineering, Wuhan Institute of Rock and Soil Mechanics, Chinese Academy of Science, Xiaohongshan, Wuchang, Wuhan 430071, China. Email: liusj2016@163.com

[6]Professor, State Key Laboratory of Geomechanics and Geotechnical Engineering, Wuhan Institute of Rock and Soil Mechanics, Chinese Academy of Science, Xiaohongshan, Wuchang, Wuhan 430071, China.

Note. This manuscript was submitted on April 13, 2018; approved on December 31, 2018; published online on April 12, 2019. Discussion period open until September 12, 2019; separate discussions must be submitted for individual papers. This paper is part of the ***International Journal of Geomechanics***, © ASCE, ISSN 1532-3641.

surface based on the definition of the safety factor through global optimization algorithms (e.g., Li and Chu 2011; Jurado-Piña and Jimenez 2015). Although these methods have a clear physical meaning for a circular or straight-line slip surface (e.g., Tang et al. 2016), some scholars (e.g., Zheng et al. 2006; Ge 2008) doubt their clarity when the critical slip surface is a noncircular slip surface because of the direction of vectors. For a noncircular slip surface, the definition of the safety factor is neither the vector sum of forces nor a projection of the algebraic sum of forces along a particular direction.

Considering the vector characteristics of force, Ge (2008) firstly put forward the vector-sum method (VSM), for which the safety factor is defined as the ratio of total resisting force to total driving force on the global sliding direction. It is known that the current stress state of the engineering object can be easily achieved from numerical analysis with any complex conditions (Lu et al. 2018a, b) and constitutive models (e.g., Tan et al. 2013, 2018), and in the past few years, this method has been developed based on the actual stress of the slope (Wu 2013; Liu et al. 2017; Fu et al. 2017). However, in the previous studies, only the force equation was considered, and the global sliding direction was still assumed based on the sliding failure mechanism. In this article, the global sliding direction is theoretically determined by the principle of potential energy minimization instead of being assumed. Moreover, the safety factor by the moment equation is established to improve the VSM. Finally, three classical soil slopes with reference solutions are used to verify the rationality and reliability of the proposed method.

Global Sliding Direction

In the previous research for VSM (Ge 2008), the global sliding direction was assumed by the shear stress under the critical state of the slope (Fig. 1). At the limiting state, there exists a list of sliding shear stress vectors distributed tangentially along the potential slip surface. The composition of these vectors yields the total sliding shear stress, which is equal to the total resisting shear stress but has a contrary sign. In consequence, if the Mohr-Coulomb yield criterion is used and the rule for the positive direction of normal stress in elastic mechanics is adopted, the global sliding direction $\mathbf{d}$ can be assumed by

$$\mathbf{d} = \frac{\int_l (c - \sigma_{nc} \tan \varphi)\mathbf{d_r} d_l}{\left\| \int_l (c - \sigma_{nc} \tan \varphi)\mathbf{d_r} d_l \right\|} \tag{1}$$

where $\mathbf{d_r}$ = unit direction of sliding shear stress at any point on the slip surface; c and φ = cohesion and friction angle of the material, respectively; σ_{nc} = normal stress at any point on the slip surface; and l = potential slip surface.

In this article, however, the global sliding direction is theoretically deduced and determined by the principle of minimum potential energy. The process is as follows.

Fig. 2 presents a simple slope. The unit weight of the slope is γ, the stress vector at any Point M of the slip surface acting on the bedrock from the sliding body is $\boldsymbol{\sigma}_\mathbf{M}$, and $\mathbf{n}$ is the normal direction at Point M. Therefore, the force equation for the sliding body can be given by

$$\int_A \mathbf{b} dA = \int_L \boldsymbol{\sigma}_\mathbf{M} dL \tag{2}$$

$$\boldsymbol{\sigma}_\mathbf{M} = \boldsymbol{\sigma} \cdot \mathbf{n} \tag{3}$$

where $\mathbf{b}$ = body force; and $\boldsymbol{\sigma}$ = stress tensor.

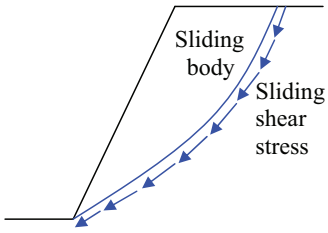

Fig. 1. Sliding shear stress at critical state.

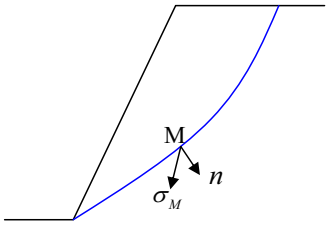

Fig. 2. Simple slope.

To demonstrate the deduction process, the sliding body with the specified slip surface is considered, and the rock or soil material under the sliding body is considered as the bedrock. Assuming the global sliding direction is $\mathbf{d}$, when the slope is about to slide, it only slides along the potential slip surface because of the restriction of the bedrock. Then, the displacement of the slope can be expressed as

$$\mathbf{d_s} = \mathbf{d} - \mathbf{d_n} = \mathbf{d} - d_n \mathbf{n} \tag{4}$$

Therefore, when the displacement of the slope is $\mathbf{d_s}$, the change of potential energy can be given by

$$\Pi = \Pi_0 + \int_S \boldsymbol{\sigma}_\mathbf{M} \cdot \mathbf{d_s} dS \tag{5}$$

Then, the first-order variation can be written as

$$\frac{\partial \Pi}{\partial \mathbf{d}} = 0 \tag{6}$$

Eq. (6) can also be considered as

$$\frac{\partial}{\partial \theta_i} \int_S \boldsymbol{\sigma}_\mathbf{M} \cdot \mathbf{d_s} dS = 0 \tag{7}$$

where $\mathbf{d} = \mathbf{d}(\theta_i)$; θ_i = independent variation of sliding direction for the 2D problem; and i is equal to 1, but for the 3D problem, it is equal to 1 and 2.

Based on Eq. (7), for the 2D problem, the sliding direction can finally be obtained as Eq. (8); the deduction process is presented in Appendix I.

$$\tan \theta = \frac{\int_l \left(n_x n_y \sigma_{Mx} + \left(n_y^2 - 1 \right) \sigma_{My} \right) dl}{\int_l \left(n_x n_y \sigma_{My} + \left(n_x^2 - 1 \right) \sigma_{Mx} \right) dl} \tag{8}$$

where σ_{Mx} and σ_{My} = components of $\boldsymbol{\sigma}_\mathbf{M}$ on the x- and y-axes.

From Eq. (8), it can be concluded that the global sliding direction can be theoretically determined by the stress state and shape of the slip slope.

Examination Example

To verify the global sliding direction determined by the principle of potential energy, Fig. 3 gives a simple sliding block. It is known that the sliding direction θ is along the inclined plane. In Fig. 3, the gravity load is only considered on the block, and the inclined angle is α.

According to Eq. (8), the components of normal direction on the x- and y-axes can be obtained as $n_x = \sin\alpha$ and $n_y = -\cos\alpha$. Similarly, the components of gravity load on the x- and y-axes can be expressed as $\sigma_{Mx} = 0$ and $\sigma_{ny} = -G$. Then, the sliding direction can be calculated by

$$\tan\theta = \frac{n_y^2 - 1}{n_x n_y} = \frac{\cos^2\alpha - 1}{\sin\alpha\cos\alpha} = \frac{-\sin^2\alpha}{\sin\alpha\cos\alpha} = -\tan\alpha \tag{9}$$

From Eq. (9), the sliding direction θ is equal to $\pi + \alpha$, which is the same direction along the inclined plane and proves that the global sliding direction by the principle of minimum potential energy is the same as the real solution for this block.

Vector-Sum Method

Because of the direction of force, the total resisting force and driving force of the potential sliding body generally have different directions. Due to different directions for both force vectors, they need to be compared in a certain direction to obtain the safety factor. Assuming there exists a global sliding direction standing for the sliding tendency of the whole sliding body, the original definition of safety factor is only with respect to the force vector equation, and the global sliding direction is just from the assumption of the supposed stress state of slope (Liu et al. 2017; Fu et al. 2017). In this section, based on the global sliding direction theoretically deduced previously, this method is supplemented by the moment equation. Based on the force vectors distributed along the potential slip surface, the sum of the resisting moment can be obtained at certain moment point, and similarly, the sum of the driving moment can also be calculated at the same moment point.

Force Vector Equation

Eq. (10) is the expression of the safety factor by force vector equation in the VSM, where F_f is the safety factor by force equation, R is the total resisting force on global sliding direction $\mathbf{d}$ (Fig. 4), T is the corresponding total driving force on the same sliding direction, l_{AB} is the potential slip surface, $\boldsymbol{\sigma}_\mathbf{M}$ is the driving stress at any Point M on the slip surface under the normal condition, and $\boldsymbol{\sigma}'_\mathbf{M}$ is the resisting stress at Point M under the critical condition.

$$F_f = \frac{R}{T} = \frac{\int_l \boldsymbol{\sigma}'_\mathbf{M} d_l \cdot \left(-\overrightarrow{\mathbf{d}}\right)}{\int_l \boldsymbol{\sigma}_\mathbf{M} d_l \cdot \mathbf{d}} \tag{10}$$

To clearly explain Eq. (10), the compositions of the driving force and resisting force are explained in the following sections.

Driving Force

Fig. 5(a) presents the stress state of a simple slope under the normal condition. In Fig. 5(a), $\mathbf{P_H}$ and $\mathbf{P_V}$ are the total horizontal and vertical forces externally acting on potential sliding body, which belong

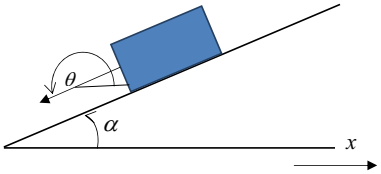

Fig. 3. Sliding block along certain inclined plane.

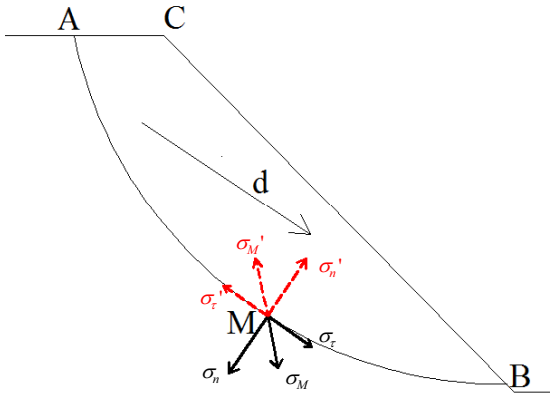

Fig. 4. Normal stress state of slope.

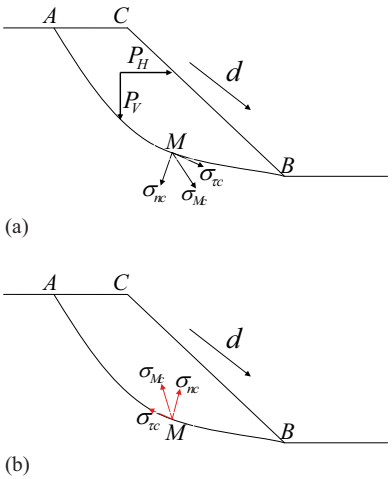

Fig. 5. Critical stress state at Point M on the slip surface: (a) driving stresses; and (b) resisting stresses.

to the forces on the macroscale; $\mathbf{d}$ is the global sliding direction; and $\boldsymbol{\sigma}_\mathbf{n}$ and $\boldsymbol{\sigma}_\boldsymbol{\tau}$ are, respectively, the normal and shear stress acting on the bedrock by the sliding body at any Point M on the potential slip surface, which belong to the stresses on the microscale for the sliding body. Thus, the total forces acting on the bedrock by the sliding body can be expressed as $\int_l (\boldsymbol{\sigma}_\boldsymbol{\tau} + \boldsymbol{\sigma}_\mathbf{n}) d_l$. According to the static balance state of the potential sliding body, Eq. (11) can be obtained based on the forces on the macroscale and stresses on the microscale.

$$\int_l (\boldsymbol{\sigma}_\boldsymbol{\tau} + \boldsymbol{\sigma}_\mathbf{n}) d_l = \mathbf{P_H} + \mathbf{P_V} \tag{11}$$

From Eq. (11), it can be seen that the forces on microscale $\int_l (\boldsymbol{\sigma}_\boldsymbol{\tau} + \boldsymbol{\sigma}_\mathbf{n}) d_l$ on the potential slip surface can be considered as the

forces on the macroscale, including all external loads acting on the potential sliding body. From the view of the forces on the macroscope, the total driving forces T should be the projection of all external loads $(\mathbf{P_V} + \mathbf{P_H})$ on the global sliding direction $\mathbf{d}$. Then, the total driving forces T can be given by

$$T = (\mathbf{P_V} + \mathbf{P_H}) \cdot \mathbf{d} \tag{12}$$

From Eqs. (11) and (12), the total driving forces can be considered as

$$T = \int_l (\boldsymbol{\sigma}_\tau + \boldsymbol{\sigma}_\mathbf{n}) d_l \cdot \mathbf{d} \tag{13}$$

Eq. (13) is the expression of total sliding forces, which is just the denominator of Eq. (10). For the VSM, the component of total driving force T is the projection of all the loads on the macroscale in the global sliding direction, which is the essential difference from conventional methods in slope stability analysis.

Resisting Force

The critical stress state of the slope presented in Fig. 5(b) is considered as an example. In Fig. 5(b), $\boldsymbol{\sigma}_{\mathbf{nc}}$ and $\boldsymbol{\sigma}_{\tau\mathbf{c}}$ are the driving normal and shear stress under the critical state at any Point M, which is shown in black color, and $\boldsymbol{\sigma}'_{\mathbf{nc}}$ and $\boldsymbol{\sigma}'_{\tau\mathbf{c}}$(gray color) are the resisting normal and shear stresses.

At the moment the slope fails, the stress state is hard to determine. However, a reasonable assumption can be made to obtain the stress under the critical state based on the failure mechanism of a landslide. As is known, the internal stress can automatically adjust to mobilize the maximum resisting capacity when the slope is about to slide along a certain slip surface. In consequence, for the slope in Fig. 4, if the slope is about to slide along the slip surface L_{AB}, the resisting force along the slip surface would be mobilized to be the maximum value. Assuming that the strength of rock and soil material complies with the Mohr-Coulomb yield criterion, the shear strength at Point M under the limiting state can be given by

$$\|\boldsymbol{\sigma}'_{\tau\mathbf{c}}\| = c + \|\boldsymbol{\sigma}'_{\mathbf{nc}}\| \tan\varphi \tag{14}$$

With respect to the direction of resisting shear stress, at the limiting state, it is opposite to the direction of slip. Thus, in Fig. 4, at Point M, only the normal stresses $\boldsymbol{\sigma}'_{\mathbf{nc}}$ and $\boldsymbol{\sigma}_{\mathbf{nc}}$ cannot be directly obtained at the limiting state. Here, it is assumed the normal stresses keep constant along the slip surface during the evolution process from the normal to limiting state.

$$\|\boldsymbol{\sigma}'_{\mathbf{nc}}\| = \|\boldsymbol{\sigma}_\mathbf{n}\| \tag{15}$$

The maximum resisting force and driving force are the pair of action and reaction. From Eqs. (13)–(15), the safety factor based on force equation can be given by

$$F_f = \frac{\int_l \left[(c + \|\boldsymbol{\sigma}_\mathbf{n}\| \tan\varphi) \dfrac{\boldsymbol{\sigma}_\tau}{\|\boldsymbol{\sigma}_\tau\|} + \boldsymbol{\sigma}_\mathbf{n} \right] d_l \cdot \mathbf{d}}{\int_l (\boldsymbol{\sigma}_\tau + \boldsymbol{\sigma}_\mathbf{n}) d_l \cdot \mathbf{d}} \tag{16}$$

It can be seen that completely different from the popular LEM and SRM, this method is a new approach to assess slope stability from the vector characteristics of force and the global mechanics analysis of the potential sliding body. Moreover, it has clear physical meaning, and based on the current stress state of the slope, the safety factor can be directly computed through stress integration along potential slip surface rather than iterative computing.

Moment Equation

Fig. 6 presents a simple slope for moment calculation, where M is any point on the slip surface, $\boldsymbol{\sigma}_\mathbf{M}$ (black color) is the driving stress vector, and $\boldsymbol{\sigma}'_\mathbf{M}$ (gray color) is the resisting stress vector. Here, Point O is assumed as the moment center, and the coordinate of the center is (a, b) in Fig. 6.

According to the definition of moment, the safety factor by the moment equation can be given by

$$F_m = \frac{-M_r}{M_d} = \frac{-\int_l (\mathbf{r} \times \boldsymbol{\sigma}'_\mathbf{M}) d_l}{\int_l (\mathbf{r} \times \boldsymbol{\sigma}_\mathbf{M}) d_l} \tag{17}$$

where F_m = safety factor by the moment equation; M_r = total resisting moment along the slip surface; and M_d = corresponding total driving moment.

The stress components of resisting plane stress can be assumed as σ'_{Mx} on the x-axis and σ'_{My} on the y-axis; correspondingly, the stress components of driving plane stress can be taken as σ_{Mx} and σ_{My}. Furthermore, the coordinates of Point M on the slip surface are considered as (x, y) in the x–y-coordinate system. Thus, Eq. (17) can be simplified as the following scalar expressions:

$$F_m = \frac{-M_r}{M_d} = \frac{\int_l \left[(y-b) \times \sigma'_{Mx} - (x-a) \times \sigma\sigma'_{My} \right] d_l}{\int_l \left[(x-a) \times \sigma_{My} - (y-b) \times \sigma_{Mx} \right] d_l} \tag{18}$$

The deduced process is given in Appendix II, and Eq. (18) is the scalar expression for the moment equation in the 2D problem. Based on the previous mechanical analysis for a potential sliding body, the safety factor by the moment equation can be easily calculated if the moment center is already determined.

Similar to the global sliding direction, the moment center is also a key issue for the moment equation [Eq. (18)]. Thus, for the VSM, the global sliding direction and moment center should be reasonably determined, or else the safety factor might be negative, which does not make sense. With respect to the center of the moment, it is difficult to determine theoretically, and in this article, it is recommended to be determined by the geometric shape of the potential slip surface, which is explained in detail in the next section.

Classic Examples

In the previous section, the force and moment equations of the VSM are demonstrated in detail. To verify the VSM, this method is

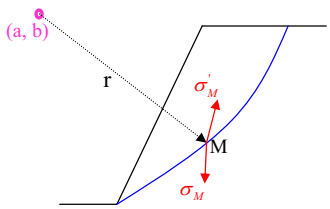

Fig. 6. Simple slope for the moment calculation.

applied to classic examples with specified slip surfaces, which have reference solutions for the slope stability.

Here, the FE method is used to get the stress field of the slope composed of elastic or elastoplastic materials. The ideal elastoplastic constitutive model, Mohr-Coulomb yield criterion, and nonassociated flow rule are used in the elastoplastic FE analysis; in addition, the dilation angle is assumed to be zero during elastoplastic FE computing. In the first two slope examples, only the self-weight of the earthen mass is considered, and for the third case, the pore pressure using the phreatic line inside the slope is taken into account. As is known, the primary characteristics of the FE method are embodied in the element stiffness matrix, which contains the geometric and material behavior information that indicates the resistance of the element to deformation when subjected to loading. The displacement of the node is first obtained by solving a matrix equation, whereas the stress, as the secondary quantity, is just expressed in terms of nodal displacement. Although the stresses at the boundary of the elements are discontinued with low accuracy, there are several recovery procedures for smoothed stress in the FE method to obtain reliable stresses on the boundary of elements (Lo and Lee 1998). After obtaining the node stress at the boundary of the element, the stress at any position within an element can be calculated by

$$\sigma = \sum_{i=1}^{n} N_i \sigma_i \tag{19}$$

$$N_i = 1/4 * (1 + \xi_i \xi)(1 + \eta_i \eta) \tag{20}$$

where n = number of nodes of the element; N_i = shape function of the nodal point i; σ_i = corresponding nodal stress; $(\xi\, \eta)$ = local coordinate at any position in an isoparametric element; and $(\xi_i\, \eta_i)$ = local coordinate of Node i in a four-node isoparametric element (Bathe 1996). It was found that any stress-smoothing technique is reliable (Lo and Lee 1998) and has almost no effect on the results by the VSM, and the errors from different smoothing techniques can be ignored.

Homogeneous Slope

This example is a slope stability benchmark example (Donald and Giam 1992) by Australia Computer Association and Design Society (ACADS), and the standard safety factor of the slope is 1.0 (i.e., the slope is a critical slope).

Calculating Conditions

The geometry of the slope is presented in Fig. 7, and the material properties of the homogenous slope are provided in Table 1. For computing conditions, the elastic model was adopted because this example is a critical slope, for which the standard safety factor is 1.00, as recognized by ACADS. For the boundary conditions, the bottom was fixed, and the lateral boundaries were normally restricted. With respect to the slip surface, the specified critical slip surface was utilized by rigorous the Morgenstern-Price method with the half-sine function as the interslice force function (Fig. 7). The calculating model of the FE analysis is presented in Fig. 8, and the total element number was 636.

Results and Analysis

First, according to the force equation [Eq. (11)], the global sliding direction of slope should be determined in advance. Based on the approaches of global sliding direction [Eqs. (1) and (8)] and the limiting stress state of the slope, the global sliding direction with different approaches can be calculated, and then the safety factor with the force vector equation can be computed.

For the moment equation of the VSM, the center of the moment should be determined before calculating the safety factor by the moment equation. The safety factor by the moment equation expresses the possibility of the rotation to the center of the moment for the sliding body, so the center of the moment is very closely related to the shape of the potential slip surface, on which the

Table 1. Material parameters

Parameter	Value
c (kPa)	3.0
φ (degrees)	19.6
γ (kN·m^{-3})	20.0
E (kPa)	1.0×10^4
μ	0.25
ψ (degrees)	0

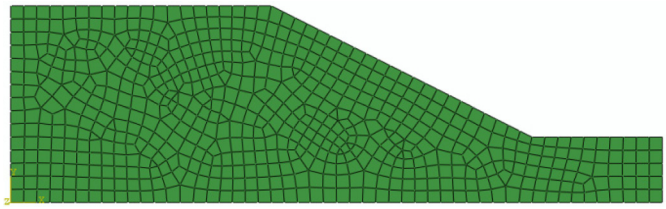

Fig. 8. Calculated model of FE analysis.

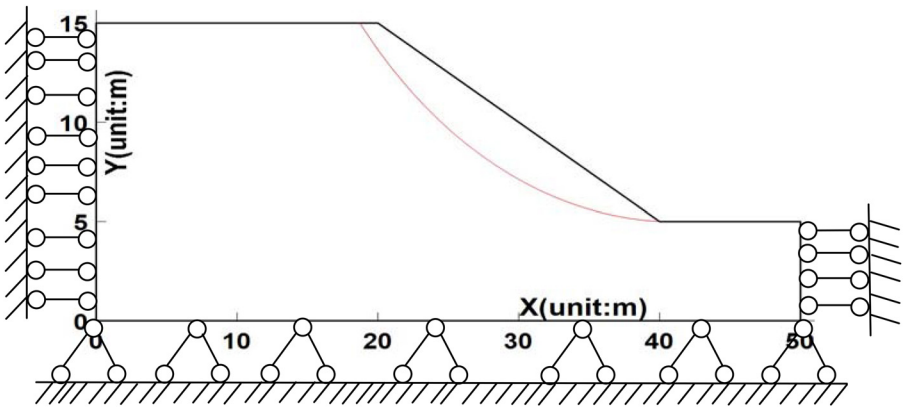

Fig. 7. Geometric model of standard example (unit: m).

Table 2. Calculated results with the VSM

Equation	Results	Value
Force equation	Safety factor	0.998
	Global sliding angle by Eq. (10) (degrees)	25.14
	Global sliding angle by Eq. (24) (degrees)	25.14
Moment equation	Safety factor	1.014
	Center of moment	(41.14, 35.09)
Reference answer	Safety factor	1.00

Note: Sliding angle is the angle between the sliding direction and the horizontal line.

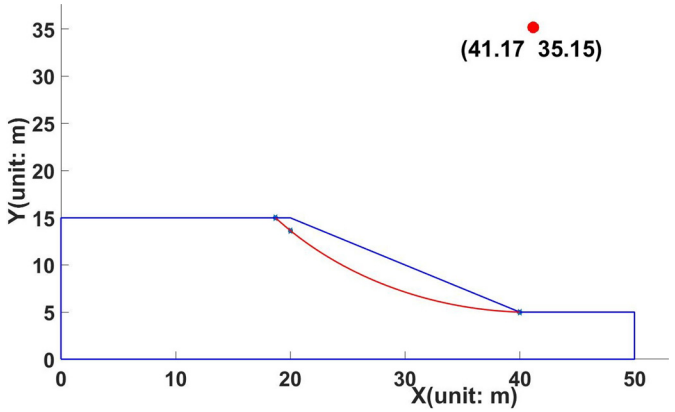

Fig. 9. Simulated circle based on any three points on slip surface.

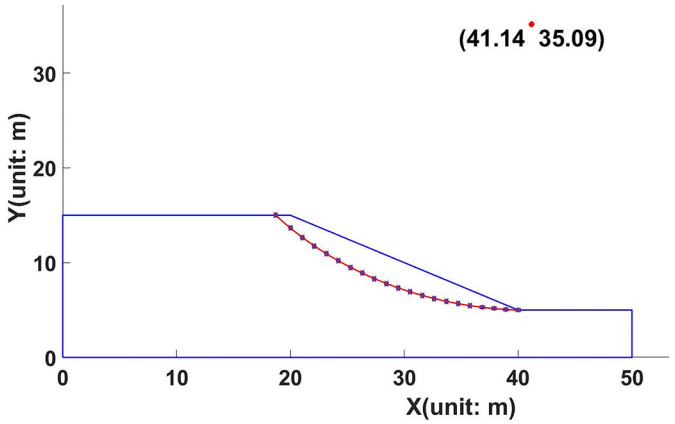

Fig. 10. Simulated circle based on most points on slip surface.

forces acting on the sliding body are distributed. Therefore, the geometric shape of a slip surface can be utilized to determine the center of the moment. For a slip surface with any shape, it is not difficult to define a circle using the key points on the slip surface, and then the center of the circle can be considered as the center of the moment.

Table 2 provides the calculated results of the VSM. It can be seen that the global sliding angle using the assumption of Eq. (1) is the same as that by the principle of minimum potential energy [Eq. (8)], which proves that the theoretical basis of the previous assumption is perfectly sound. As provided in Table 2, the safety factors are consistent with the reference solution. For the force equation, it is 0.998, which is slightly less than the reference safety factor of 1.0, and it is 1.014 for the moment equation, which is slightly more than 1.0.

For the center of the moment, it is straightforward to use the points on the slip surface for defining a circle. The circle center can be considered as the center of the moment. Fig. 9 presents the simulated result using only three key points on slip surface, and the circle center is at the location (41.17, 35.15). Additionally, as a comparison, most points on the slip surface were used to simulate a circle, which is presented in Fig. 10. The moment center is at the location (41.14, 35.09), which is almost at the same location as the center using only three points on the slip surface. It can be concluded that for a circular slip surface, any three points can be used to reasonably decide the center of the moment.

Nonhomogeneous Slope with Circular Slip Surface

This example is from the Talbingo Dam in Australia and was also collected by ACADS. Fig. 11 presents the geometry of the dam; the dashed line is the specified circular slip surface. Table 3 gives the locations of key points in Fig. 11. Based on the key locations of the dam, the center of the circular slip surface was confirmed at (100.3, 290) by ACADS, and the radius of the circle is 278.8 m (Chen 2003). According to the key locations of the dam, the calculated model with FE analysis was established (Fig. 12).

Table 4 provides the parameters of the rockfill materials. For the boundary conditions of the calculated model, only the bottom was fixed, and other boundaries were free. Based on the process of the VSM, the safety factors can be obtained by the force and moment equations in this method, as provided in Table 5. Because the VSM is based on only the stress state of the dam, the elastic stress state and elastoplastic stress state with the dilation angle 0°can be used to estimate the stability of the dam. The calculated results show that the plastic zone only occurred in the shallow skin of the dam, and

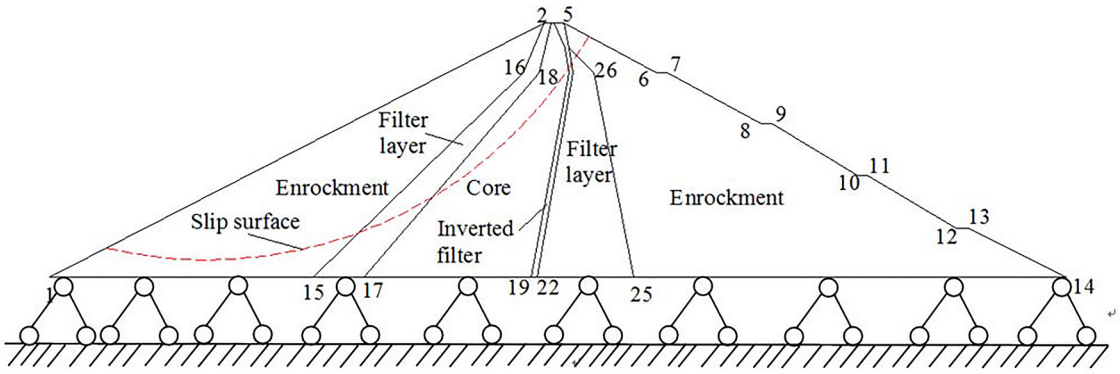

Fig. 11. Geometry of the Talbingo Dam.

the safety factors are consistent using both the elastic stress state and elastoplastic stress state of the dam. Table 5 provides the results under the elastic stress state.

From the calculated results, it can be seen that the safety factor with the moment equation is 2.33, slightly greater than the reference solution of 2.29 given by ACADS. However, the safety factor with the force equation is approximately 2.497, remarkably greater than the reference solution. For this dam, the safety factor with the moment equation controls the stability rather than that by the force equation. Furthermore, the global sliding directions are also the same by both the previous assumption and the principle of minimum potential energy.

Table 3. Coordinates of key points

Number of points	X (m)	Y (m)
1	0.0	0.0
2	315.5	162.0
3	319.5	162.0
4	321.6	162.0
5	327.6	162.0
6	386.9	130.6
7	394.1	130.6
8	453.4	97.9
9	460.6	97.9
10	515	65.3
11	521.1	65.3
12	577.9	31.4
13	585.1	31.4
14	648	0.0
15	168.1	0.0
16	302.2	130.6
17	200.7	0.0
18	311.9	130.6
19	307.1	0.0
20	331.3	130.6
21	328.8	146.1
22	310.7	0.0
23	333.7	130.6
24	331.3	146.1
25	372.4	0.0
26	347.0	130.6

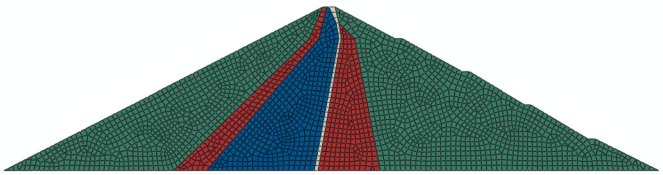

Fig. 12. Calculated model of FE analysis.

Slope with a Subhorizontal Weak Band and Varying Phreatic Line

This problem was originally studied by Giam and Donald (1989) with a slope incorporating a thin, steeply dipping weak soil layer and a variable water table. Additionally, it is an unstable slope with a factor of safety less than 1.0. In 2014, with the aim of using a strength-reduction FE program for this problem, the slope was updated, and the loading from the crest was removed; moreover, the strength of the weak band was increased to create an initially stable slope (Matthews et al. 2014).

Calculating Conditions

This slope was used to test the ability of the proposed procedure for a noncircular slip surface. The geometry, phreatic line, and strata are presented in Fig. 13. Based on the geometry of this slope, the calculated model of the FE analysis was established (Fig. 14), with a total element number of 1,744. For the boundary conditions of the calculated model, the bottom was fixed, the lateral was pinned, and the other boundaries were free. Table 6 provides the parameters of the slope materials.

Results and Analysis

According to the theory of the VSM in the previous section, the stress state of the slope using FE analysis has to be obtained, and for this slope, the ideal elastoplastic constitutive model, Mohr-Coulomb yield criterion, and nonassociated flow rule were used in the elastoplastic FE analysis. Due to the influence of a weak band inside the slope, the stability of this slope is controlled by a noncircular slip surface. The critical noncircular slip surface was determined by the previous study presented in Fig. 15, and the key points along the slip surface from the crest to the front edge are listed in Table 7. The calculated results are provided in Table 8. It can be seen that the global sliding angle is 24.56°, the center of the moment is at the location (30.68, 46.19) (Fig. 16), and the safety factors using the force and moment equations are 1.097 and 1.153.

The calculated results for this slope with different methods are summarized in Table 9. From these results, it can be seen that for a noncircular slip surface, the safety factor determined by the FE analysis is slightly greater than that by any other method, and the safety factors by the proposed method are in good agreement with

Table 5. Calculated results with the VSM

Equation	Result	Value
Force equation	Safety factor	2.497
	Global sliding angle by Eq. (10) (degrees)	18.66
	Global sliding angle by Eq. (24) (degrees)	18.66
Moment equation	Safety factor	2.33
	Center of moment	(100.3, 290)
Reference answer	Safety factor	2.29

Note: Sliding angle is the angle between the sliding direction and the horizontal line.

Table 4. Materials parameters

Material	c (kPa)	φ (°)	ψ (°)	γ (kN·m^{-3})	E [kPa ($\times 10^4$)]	μ	ψ (°)
Enrockment	0.0	45	0.0	20.4	5.0	0.30	0
Filter layer	0.0	45	0.0	20.4	5.0	0.30	0
Inverted layer	0.0	45	0.0	20.4	4.0	0.30	0
Core	85.0	23	0.0	18.1	1.0	0.44	0

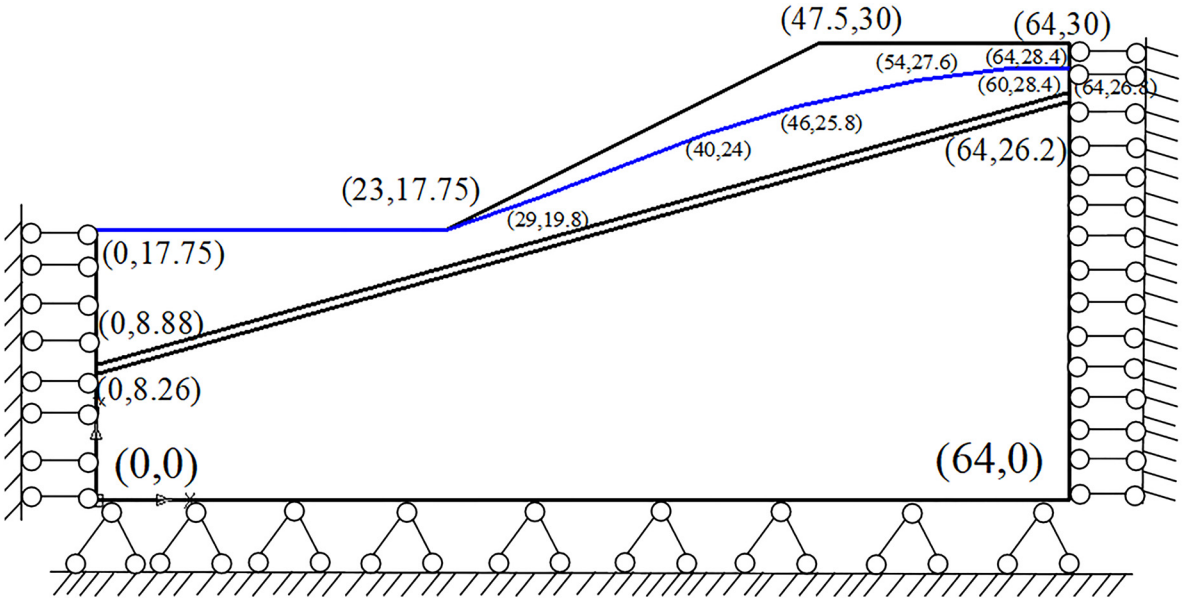

Fig. 13. Geometry of the slope with a subhorizontal weak band and varying phreatic line.

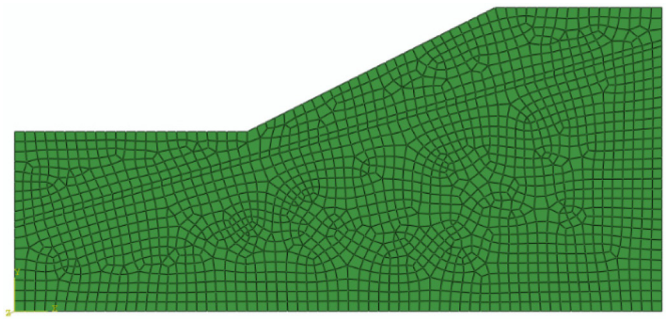

Fig. 14. FE calculated model of the slope.

Table 6. Material parameters

Material	Cohesion [c (kPa)]	Friction angle [φ (°)]	Dilation angle [ψ (°)]	Density [γ (kN·m^{-3})]	Young's modulus [E (kPa)]	Poisson's ratio (μ)
Soil 1	20.0	28.5	0.0	18.84	1.0e2	0.30
Soil 2	10.0	15.0	0.0	18.84	1.0e2	0.30

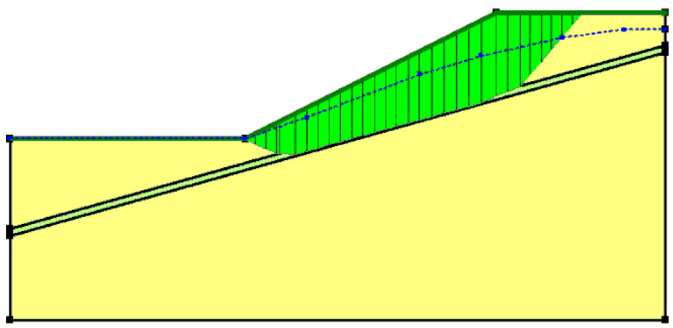

Fig. 15. Noncircular slip surface determined by Matthews et al. (2014).

Table 7. Coordinates of key points for noncircular slip surface

X (m)	Y (m)
22.69	17.75
26	16.25
27.90	16.20
46	21.20
49.80	22.80
56	30

Table 8. Calculated results with the VSM for noncircular slip surface

Equation	Result	Value
Force equation	Safety factor	1.097
	Global sliding angle by Eq. (10) (degrees)	20.555
	Global sliding angle by Eq. (24) (degrees)	20.555
Moment equation	Safety factor	1.153
	Center of moment	(30.68, 46.19)

those by the rigorous Morgenstern-Price method. It can be concluded that any method in Table 9 can assess the stability of this slope.

Discussion

1. In the conventional methods for slope stability analysis, the safety factor of the slope is calculated using the iterative algorithm in a force equilibrium or moment equilibrium equation. However, considering the vector characteristics of force, the VSM can directly assess the stability of the slope using force and moment equations based on the global sliding direction and the center of the moment. Although the calculated results of classic examples verified the VSM for the 2D problem, further study of 3D problems is necessary.
2. For the FE strength-reduction technique in slope stability analysis, much computational time is demanded because reiterative computing with different strength parameters is required until

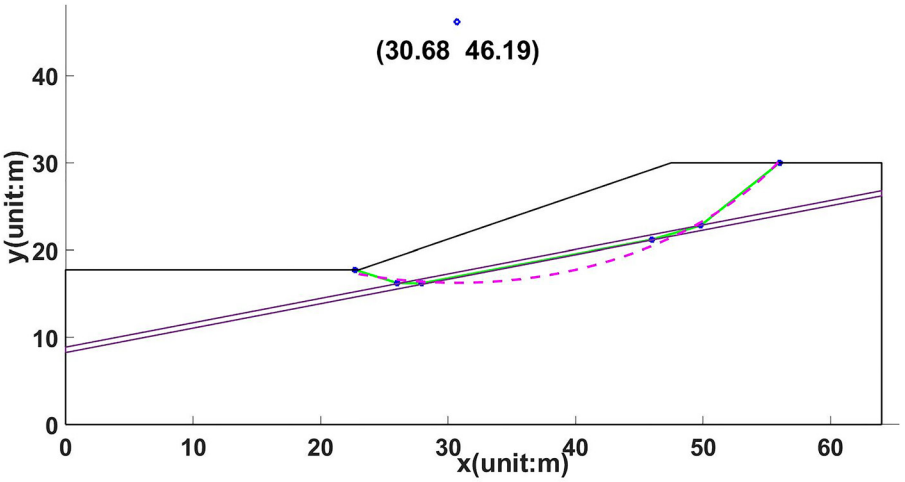

Fig. 16. Center of moment using key points.

Table 9. Comparison of results with different methods for the slope

Method	Safety factor
FE analysis	1.181
Limit-equilibrium method	1.112
Vector-sum method	
Force equation	1.097
Moment equation	1.153

the slope reaches the critical state, and assessment of the stability is thus a time-consuming process, especially in a 3D problem with complex conditions. The VSM can overcome this drawback because the stress field is easily obtained by numerical analysis and because of the simple calculation of the safety factor based on the stress field of the slope. However, it is still necessary to search the critical slip surface, just like in the methods based on the stress state of the sliding body mentioned in the Introduction.

3. The global sliding direction is the key issue in the VSM. In this study, the global sliding direction was deduced by the principle of minimum potential energy, which provides a rigorous theory to solve this issue. In addition, for the three cases shown previously, it is very interesting that the sliding directions found by the previous assumption are the same as those found by this theory. Because the ultimate stress state of the slope is unknown, it has to be assumed based on the potential sliding failure mode and mechanical characteristics under the ultimate state in practical engineering [Eq. (1)]. Meanwhile, as shown in Eq. (9), the sliding direction deduced by this theory still depends on the stress state and the geometric shape of the slope. Therefore, this interesting phenomenon is rooted in the same ultimate stress state of the slope from practical engineering knowledge and the potential sliding failure mode of the slope. Thus, a thorough mastery of the potential sliding failure mode and mechanism of the slope is of significance to perform the slope stability analysis.

Conclusion

1. Compared with existing methods in slope stability analysis, the highlight of the proposed VSM is that it considers both the magnitude and direction of the force in the global sliding direction rather than only the scalar characteristics of the force as in other methods. Moreover, this method directly compares the projection of the total resisting force with the total sliding force in the global sliding direction and compares the resisting moment with the driving moment at the center of the moment. It thus has clear physical meaning for a slip surface of any shape and can be used to compute the factor of safety explicitly. Additionally, the slope with complex conditions can be directly assessed by this method based on only the actual stress state of the slope found by any numerical analysis method.
2. This article emphasizes the sliding direction using the principle of minimum potential energy, which supplies rigorous theory for the global sliding direction. In addition, the moment equation of the VSM is still put forward, which improves this method.
3. The VSM was applied in classic examples with specified slip surfaces. The calculated results show that the safety factors of the VSM are consistent with the reference solutions, which demonstrates the accuracy of the VSM.

Appendix I. Deduced Process of Sliding Direction

In Eq. (2), $\mathbf{b}$ is the body force, and $\boldsymbol{\sigma}$ is the stress tensor. For a 2D problem, they can be expressed as

$$\mathbf{b} = \begin{bmatrix} 0 \\ \gamma \end{bmatrix} \tag{21}$$

$$\boldsymbol{\sigma} = \begin{bmatrix} \sigma_x & \tau_{xy} \\ \tau_{xy} & \sigma_y \end{bmatrix} \tag{22}$$

And for a 3D problem, they can be expressed as

$$\mathbf{b} = \begin{bmatrix} 0 \\ 0 \\ \gamma \end{bmatrix} \tag{23}$$

$$\boldsymbol{\sigma} = \begin{bmatrix} \sigma_x & \tau_{xy} & \tau_{xz} \\ \tau_{xy} & \sigma_y & \tau_{yz} \\ \tau_{xz} & \tau_{yz} & \sigma_z \end{bmatrix} \tag{24}$$

For a 2D problem, the global sliding direction can be expressed by the sliding angle θ as

$$\mathbf{d} = \begin{bmatrix} \cos\theta \\ \sin\theta \end{bmatrix} \tag{25}$$

where θ = sliding angle, defined as the inclined angle from the x-axis to the global sliding direction. Then, the displacement of the slope $\mathbf{d_s}$ can be expressed as

$$\mathbf{d_s} = \mathbf{d} - d_n\mathbf{n} = \begin{bmatrix} \cos\theta \\ \sin\theta \end{bmatrix} - \left(\begin{bmatrix} n_x & n_y \end{bmatrix} \begin{bmatrix} \cos\theta \\ \sin\theta \end{bmatrix} \right) \begin{bmatrix} n_x \\ n_y \end{bmatrix} \tag{26}$$

That is

$$\mathbf{d_s} = \mathbf{d} - d_n\mathbf{n} = \begin{bmatrix} 1 - n_x^2 & -n_x n_y \\ -n_x n_y & 1 - n_y^2 \end{bmatrix} \begin{bmatrix} \cos\theta \\ \sin\theta \end{bmatrix} \tag{27}$$

Eq. (27) is substituted into Eq. (7), giving

$$\int_l \begin{bmatrix} \sigma_{Mx} & \sigma_{My} \end{bmatrix} \begin{bmatrix} n_x^2 - 1 & n_x n_y \\ n_x n_y & n_y^2 - 1 \end{bmatrix} \begin{bmatrix} \sin\theta \\ -\cos\theta \end{bmatrix} dl = 0 \tag{28}$$

where σ_{Mx} and σ_{My} = components of $\boldsymbol{\sigma}_\mathbf{M}$ on the x- and y-axes. The equation can be simplified, and the sliding direction can be finally obtained as Eq. (9).

Appendix II. Deduced Process of Moment Equation

According to the definition of a moment, the magnitude of the moment of the acting force at a certain point is directly proportional to the distance from the point to the force. It is defined as the cross product of the acting force vector $\mathbf{F}$ and the distance vector $\mathbf{r}$, and based on the right-hand rule, the moment can be calculated by

$$\boldsymbol{M} = \mathbf{r} \times \boldsymbol{F} \tag{29}$$

where distance vector $\mathbf{r}$ = vector from the moment point to the acting point of the force. For the simple slope in Fig. 6, the resisting moment at Point M on a slip surface can be calculated as

$$\boldsymbol{M_r} = \mathbf{r} \times \boldsymbol{\sigma}'_{\boldsymbol{M}} \tag{30}$$

Similarly, the driving moment at Point S can be obtained by

$$\boldsymbol{M_d} = \mathbf{r} \times \boldsymbol{\sigma}_M \tag{31}$$

For a 2D problem, the scalar expression can be deduced. Thus, Eqs. (27) and (28) can be simplified as the following scalar expressions:

$$M_r = \mathbf{r} \times \boldsymbol{\sigma}'_\mathbf{M} = \sigma'_{My} \times (x - a) - \sigma'_{Mx} \times (y - b) \tag{32}$$

$$M_{Sd} = \mathbf{r} \times \boldsymbol{\sigma}_\mathbf{S} = \sigma_{sy} \times (x - a) - \sigma_{sx} \times (y - b) \tag{33}$$

Therefore, the safety factor by the moment equation can be finally obtained as Eq. (19).

Acknowledgments

The authors gratefully acknowledge the financial support of the China Scholarship Council and National Natural Science Foundation of China (Grant 51674239), Open Funds Research Project of Key Laboratory of Geological Hazards on Three Gorges Reservoir Area (China Three Gorges University), Ministry of Education (2018KDZ02), and International Science and Technology Cooperation Program of China (Grant 2018YFE0100100). We further thank two anonymous reviewers, the associate editor, and editorial coordinator Monica Leigh for their valuable comments, which improved this article significantly.

References

Bathe, K.-J. 1996. *Finite element procedures*. Upper Saddle River, NJ: Prentice-Hall.

Bishop, A. W. 1955. "The use of the slip circle in the stability analysis of slopes." *Géotechnique* 5 (1): 7–17. https://doi.org/10.1680/geot.1955.5.1.7.

Chakraborty, A., and D. Goswami. 2016. "State of the art: Three dimensional (3D) slope-stability analysis." *Int. J. Geotech. Eng.* 10 (5): 493–498. https://doi.org/10.1080/19386362.2016.1172807.

Chen, Z. 2003. *Earth slope stability analyses—Theory, method and programs*. [In Chinese.] Beijing: China Water Power.

Cheng, Y. M., T. Lansivaara, and W. B. Wei. 2007. "Two-dimensional slope stability analysis by limit equilibrium and strength reduction methods." *Comput. Geotech.* 34 (3): 137–150. https://doi.org/10.1016/j.compgeo.2006.10.011.

Cheng, Y. M., and C. J. Yip. 2007. "Three-dimensional asymmetrical slope stability analysis extension of Bishop's, Janbu's, and Morgenstern–Price's techniques." *J. Geotech. Geoenviron. Eng.* 133 (12): 1544–1555. https://doi.org/10.1061/(ASCE)1090-0241(2007)133:12(1544).

Donald, I. B., and P. S. K. Giam. 1992. "The ACADS slope stability programs review." In Vol. 3 of *Proc., 6th Int. Symp. on Landslides*, edited by D. H. Bell, 1665–1670. Amsterdam, Netherlands: Elsevier.

Duncan, J. M. 1996. "State of the art: Limit equilibrium and finite-element analysis of slopes." *J. Geotech. Eng.* 122 (7): 577–596. https://doi.org/10.1061/(ASCE)0733-9410(1996)122:7(577).

Fredlund, D. G., and J. Krahn. 1977. "Comparison of slope stability methods of analysis." *Can. Geotech. J.* 14 (3): 429–439. https://doi.org/10.1139/t77-045.

Fu, X., Q. Sheng, Y. Zhang, J. Chen, S. Zhang, and Z. Zhang. 2017. "Computation of the safety factor for slope stability using discontinuous deformation analysis and the vector sum method." *Comput. Geotech.* 92: 68–76. https://doi.org/10.1016/j.compgeo.2017.07.026.

Ge, X. R. 2008. "Deformation control law of rock fatigue failure, real-time X-ray CT scan of geotechnical testing, and new method of stability analysis of slopes and dam foundations." [In Chinese.] *Chin. J. Geotech. Eng.* 30 (1): 1–20.

Giam, P. S. K., and I. B. Donald, 1989. *Example problems for testing soil slope stability programs*. Civil Engineering Research Rep. No. 8/1989. Melbourne, Australia: Monash Univ.

Griffiths, D. V., and P. A. Lane. 1999. Slope stability analysis by finite elements. *Géotechnique* 49 (3): 387–403. https://doi.org/10.1680/geot.1999.49.3.387.

Janbu, N. 1973. "Slope stability computations." In *Embankment-Dam engineering: Casagrande volume*, 47–86. New York: Wiley.

Jurado-Piña, R., and R. Jimenez. 2015. "A genetic algorithm for slope stability analyses with concave slip surfaces using custom operators." *Eng. Optim.* 47 (4): 453–472. https://doi.org/10.1080/0305215X.2014.895339.

Lam, L., and D. G. Fredlund. 1993. "A general limit equilibrium model for three-dimensional slope stability analysis." *Can. Geotech. J.* 30 (6): 905–919. https://doi.org/10.1139/t93-089.

Li, L., and X. Chu. 2011. "An improved particle swarm optimization algorithm with harmony strategy for the location of critical slip surface of slopes." *China Ocean Eng.* 25 (2): 357–364. https://doi.org/10.1007/s13344-011-0030-9.

Liu, G., X. Zhuang, and Z. Cui. 2017. "Three-dimensional slope stability analysis using independent cover based numerical manifold and vector method." *Eng. Geol.* 225: 83–95. https://doi.org/10.1016/j.enggeo.2017.02.022.

Lo, S. H., and C. K. Lee. 1998. "On using different recovery procedures for the construction of smoothed stress in finite element method." *Int. J. Numer. Methods Eng.* 43 (7): 1223–1252. https://doi.org/10.1002/(SICI)1097-0207(19981215)43:7<1223::AID-NME466>3.3.CO;2-K.

Lu, Z., R. Fang, H. Yao, C. Dong, and S. Xian. 2018a. "Dynamic responses of unsaturated half-space soil to a moving harmonic rectangular load." *Int. J. Numer. Anal. Methods Geomech.* 42 (9): 1057–1077. https://doi.org/10.1002/nag.2780.

Lu, Z., R. Fang, H. Yao, Z. Hu, and J. Liu. 2018b. "Evaluation and analysis of the traffic load–induced settlement of roads on soft subsoils with low embankments." *Int. J. Geomech.* 18 (6): 04018043. https://doi.org/10.1061/(ASCE)GM.1943-5622.0001123.

Matthews, C., Z. Farook, and P. R. Helm. 2014. "Slope stability analysis—Limit equilibrium or the finite element method?" *Ground Eng.* 48 (5): 22–28.

Morgenstern, N. R., and V. E. Price. 1965. "The analysis of the stability of general slip surface." *Géotechnique* 15 (1): 79–93. https://doi.org/10.1680/geot.1965.15.1.79.

Shen, J., and M. Karakus. 2014. "Three-dimensional numerical analysis for rock slope stability using shear strength reduction method." *Can. Geotech. J.* 51 (2): 164–172. https://doi.org/10.1139/cgj-2013-0191.

Sloan, S. W. 2013. "Geotechnical stability analysis." *Géotechnique* 63 (7): 531–571. https://doi.org/10.1680/geot.12.RL.001.

Spencer, E. 1967. "A method of analysis of embankments assuming parallel inter-slice forces." *Géotechnique* 17 (1): 11–26. https://doi.org/10.1680/geot.1967.17.1.11.

Stianson, J. R., D. G. Fredlund, and D. Chan. 2011. "Three-dimensional slope stability based on stresses from a stress-deformation analysis." *Can. Geotech. J.* 48 (6): 891–904. https://doi.org/10.1139/t11-006.

Tan, X., W. Chen, H. Lui, L. Wang, W. Ma, and A. H. C. Chan. 2018. "A unified model for frost heave pressure in the rock with a penny-shaped fracture during freezing." *Cold Reg. Sci. Technol.* 153: 1–9. https://doi.org/10.1016/j.coldregions.2018.04.016.

Tan, X., W. Chen, G. Wu, and J. Yang. 2013. "Numerical simulations of heat transfer with ice–water phase change occurring in porous media and application to a cold-region tunnel." *Tunnelling Underground Space Technol.* 38: 170–179. https://doi.org/10.1016/j.tust.2013.07.008.

Tang, H., X. Lui, C. Xiong, Z. Wang, and M. A. M. Ez Eldin. 2016. "Proof of nondeterministic polynomial-time complete problem for soil slope-stability evaluation." *Int. J. Geomech.* 16 (5): C4015004. https://doi.org/10.1061/(ASCE)GM.1943-5622.0000595.

Wu, Z. 2013. "New analysis method for slope stability considering force-vector characteristics." *J. Geotech. Geoenviron. Eng.* 139 (10): 1813–1816. https://doi.org/10.1061/(ASCE)GT.1943-5606.0000905.

Zheng, H. 2012. "A three-dimensional rigorous method for stability analysis of landslides." *Eng. Geol.* 145–146: 30–40. https://doi.org/10.1016/j.enggeo.2012.06.010.

Zheng, H., L. G. Tham, and D. Liu. 2006. "On two definitions of the factor of safety commonly used in the finite element slope stability analysis." *Comput. Geotech.* 33 (3): 188–195. https://doi.org/10.1016/j.compgeo.2006.03.007.

Zhou, X. P., and H. Chen. 2013. "Analysis of stability of three-dimensional slopes using the rigorous limit equilibrium method." *Eng. Geol.* 160: 21–33. https://doi.org/10.1016/j.enggeo.2013.03.027.

Zhu, D. Y., and Q. Qian. 2007. "Rigorous and quasi-rigorous limit equilibrium solutions of 3D slope stability and application to engineering." *Chin. J. Rock Mech. Eng.* 26 (8): 1513–1528.

Zhu, D. Y., C. F. Lee, and H. D. Jiang. 2003. "Generalised framework of limit equilibrium methods for slope stability analysis." *Géotechnique* 53 (4): 377–395. https://doi.org/10.1680/geot.2003.53.4.377.

Zienkiewicz, O. C., C. Humpheson, and R. W. Lewis. 1975. "Associated and non-associated visco-plasticity in soil mechanics." *Géotechnique* 25 (4): 671–689. https://doi.org/10.1680/geot.1975.25.4.671.

Zou, J. Z., D. J. Williams, and W. L. Xiong. 1995. "Search for critical slip surfaces based on finite element method." *Can. Geotech. J.* 32 (2): 233–246. https://doi.org/10.1139/t95-026.